Environmental Science & Technology

pubs.acs.org/est

Article

Canopy-Level Flux and Vertical Gradients of Hg^0 Stable Isotopes in Remote Evergreen Broadleaf Forest Show Year-Around Net Hg^0 Deposition

Bo Wang, Wei Yuan, Xun Wang, Kai Li, Che-Jen Lin, Ping Li, Zhiyun Lu, Xinbin Feng,* and Jonas Sommar*

Cite This: *Environ. Sci. Technol.* 2022, 56, 5950−5959

Read Online

ACCESS | Metrics & More | Article Recommendations | Supporting Information

ABSTRACT: Vegetation uptake represents the dominant route of Hg input to terrestrial ecosystems. However, this plant-directed sink is poorly constrained due to the challenges in measuring the net Hg^0 exchange on the ecosystem scale over a long period. Particularly important is the contribution in the subtropics/tropics, where the bulk (~70%) of the Hg^0 deposition is considered to occur. Using the relaxed eddy accumulation technique, this study presents for the first time a whole ecosystem Hg^0 flux record over an evergreen hardwood forest. This tower-based micrometeorological method gauged a cumulated net Hg^0 flux of −41.1 $\mu g\ m^{-2}$ over 16 months, suggesting that the subtropical montane forest acts as a large and continuous sink of atmospheric Hg^0. The monthly net fluxes were consistently negative (−7.3 to −1.0 $\mu g\ m^{-2}\ month^{-1}$) throughout the year, with the smallest absolute values occurring during the mild and dry subseason in spring, which was also the annual lowest in vegetation activity. Colocated measurements of multilevel gradients of Hg^0 concentration and its stable isotopic composition support the finding of year-round Hg^0 deposition. The stable Hg isotope measurements also show that in-canopy bi-directional Hg^0 exchange is prevalent.

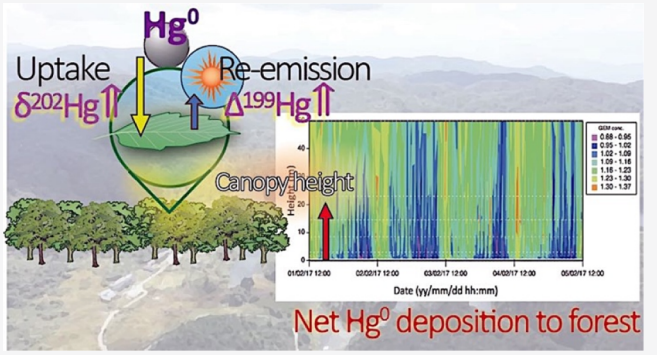

KEYWORDS: *Hg^0 exchange, micrometeorological method, atmospheric Hg^0, Hg^0 isotopes, subtropic forest*

1. INTRODUCTION

Mercury (Hg) is a bioaccumulative global contaminant that is covered by the UN's Minamata Convention (UN-MC), which came into force in 2017 with the goal of reducing Hg use and its release to the atmosphere. A central biogeochemical feature of Hg consists of dynamic deposition and re-emission cycles that atmospheric Hg dominated by gaseous elemental form (Hg^0, >95%) continuously passes through after it is released into the atmosphere. Poor constraints on the budget and mechanisms of Hg^0 exchange between land and atmosphere limit the possibilities for assessing the efficacy of global emission reduction measures.[1] Among land-atmosphere exchanges of Hg^0, forest ecosystems have the largest uncertainties (−727 to 707 Mg yr^{-1})[2] due to a paucity of whole-ecosystem studies providing seasonal flux information and uncertain contributions of leaf-atmosphere exchanges.[1,3−5] It has nevertheless been recognized that foliar Hg^0 uptake may dominate Hg input to vegetated ecosystems compared with dry deposition by gaseous and particle-bound Hg^{II} (GOM and PBM, respectively) and wet Hg^{II} deposition.[6−9] The former process may sequester ~20% of the global Hg^0 atmospheric pool and explain its seasonal variations.[10] However, Hg^0 exhibits bidirectional exchange at air−leaf interfaces as the net flux at any time may represent the combination of opposing component fluxes.[11]

By measuring Hg stable isotopic ratios in biomass, flux, and air through branch-level experiments, we have shown that maturing foliage progressively assimilates Hg^0, while re-emission derived from previously sequestered Hg occurs continuously at a weaker intensity (~30% on average) in an evergreen broadleaf (EB) forest of Southwest China (Mt. Ailao).[6,12] Based on the observed extent of Hg^0 re-emission to uptake, the gross foliar Hg^0 uptake flux exceeds previous global assessments.[10,13] Because different forest types display unequaled features in Hg input, assimilation, and transformation, the upscaling of spatially limited data is necessarily crude and warrants further study. In particular, EB forests of Southwest

Received: January 30, 2022
Revised: March 28, 2022
Accepted: April 5, 2022
Published: April 14, 2022

https://doi.org/10.1021/acs.est.2c00778
Environ. Sci. Technol. 2022, 56, 5950−5959

China with a year-round growing season experience an elevated Hg input dominated by litterfall that may rival the quantities observed in temperate/boreal (T/B) forests by up to one order of magnitude.[14−17] It is suggested that these large differences mainly stem from a combined effect of divergent litter biomass production, leaf lifespan, and stomatal conductance for Hg^0 uptake during leaf growth.[17] In addition, the old-growth EB canopies of Mt. Ailao supply substantial through-fall deposition fluxes that have been proposed to be linked to the PBM dry deposition onto foliage followed by partial wash-off.[18,19] There is a steady Hg accumulation in decomposing litter biomass, indicating that the forest floor is a consistent Hg sink.[20] The seasonal series of branch-level flux measurements suggest that the EB canopy is a general sink for atmospheric Hg^0.[12,21]

Nevertheless, there are differences in foliar Hg^0 uptake within the small sample of tree species that were examined.[22,23] Hence, the biodiversity and the complex 3D structure of canopies make it unfeasible to extrapolate net exchange processes based only on spatially confined branch-level observations in any representative manner to forest-atmosphere net exchange at an ecosystem scale, of which micrometeorological-based (MM) flux measurement methods covering a large footprint over the forest canopy are better suited.[24] It is also anticipated that further Hg^0 depositions occur via woody tissues,[25−27] cryptogamic covers,[9,28,29] and throughfall,[30,31] which is not accounted for by branch-level chamber measurements.[12,21,22] Using eddy covariance (EC, an MM technique), it has been established that the Mt. Ailao EB forest acts as a continuously large CO_2 sink over the full year.[32,33] Worldwide, the few long-term MM Hg^0 flux measurements over forests show that the magnitude and direction of fluxes are seasonally dynamic, with an overall growing period net deposition observed over rural deciduous forests in New England[34,35] and the net emission over pollution impacting coniferous forests in China.[36] For rural forest sites, significantly low or seasonally near-depleted ambient air Hg^0 concentrations have been observed.[14,21,37−39] At the latter site, measured vertical gradients of decreasing Hg^0 concentration from above the canopy to in the canopy toward the forest floor correlate with a more augmented, heavy Hg isotope composition (positive shift in $\delta^{202}Hg^0$) in the canopy air.[14,40] Required for CO_2 in forests, such profile measurements should be considered to constrain the time-resolved net ecosystem exchange (NEE) of Hg^0 because on a diel basis, the contribution from both vertical flux and storage flux may necessitate quantification.[41]

The primary objective of this study was to quantitatively constrain whether the EB forest ecosystem is a net source or sink of atmospheric Hg^0 with a method that is independent of traditional bottom-up approaches being implemented as well.[42] Using an eddy flux tower platform, we applied the above-canopy MM-flux technique and vertical Hg^0 concentration profile measurements in the air space underneath to quantify the Hg^0 NEE of a pristine old-growth EB forest near the summit of Mt. Ailao. In addition, isotopic profile measurements of Hg^0 were employed as tracers for foliar Hg^0 uptake (positive shift in $\delta^{202}Hg^0$) and re-emission (positive shift in $\Delta^{199}Hg^0$).

2. MATERIALS AND METHODS

2.1. Experimental Site. Mt. Ailao in the Xujiaba region of Yunnan Province, Southwest China, is one of the largest tracts (504 km^2) of native evergreen broadleaved forest in China.[43] Hg^0 flux and vertical concentration profile measurements were conducted during the period 2016−2018 using a 55 m tall eddy flux tower in an evergreen broad-leaved forest at 2400 m a.s.l. with canopy heights in the range of 18−26 m and a biomass of 466 tons ha^{-1} belonging to the Ailaoshan Station for Subtropical Forest Ecosystem Research Studies (ASSFERS, 24°32′N, and 101°01′E). The local leaf area index (LAI) was determined to be 3.8 m^2 m^{-2}, with the highest leaf area density occurring between 8 and 13 m (Figure S1). Vegetation activity, inferred from the local normalized difference vegetation index (NVDI, 0.6−0.8), is relatively consistent throughout the year.[40] The dominant tree species include *Lithocarpus xylocarpus*, *Castanopsis wattii*, *Schima noronhae*, *Fargesia nitida*, and *Plagiogyria communis*.[44] The montane site experiences a subtropical cool and moist climate driven by Indian and East Asian monsoons and a pronounced dry season during the period from December to April. The sunshine duration in the wet season is much shorter than that in the dry season, with a minimum of clear skies during the moist period from June to July.[45]

2.2. Vertical Hg^0 Concentration and Isotope Profile Measurements. During continuous cycles, Hg^0 concentrations were measured sequentially from six logarithmically scaled heights within the canopy [0.5 m (z_1), 1.7 m (z_2), 3.0 m (z_3), 5.0 m (z_4), 8.5 m (z_5), and 14.6 m (z_6)], one level at the canopy [25 m (z_7)] and one level adjacent to Hg^0 MM flux measurements [45 m (z_8)] using a Tekran model 2537A analyzer coupled via a Tekran model 1115 synchronized multiport manifold (Tekran Inc., Canada). The manifold switching interval was set to 10 min, yielding two samples of 3.75 L from each port during a cycle of 80 min. The manifold was configured to allow the deactivated ports to be continually flushed by a bypass pump (model R155-V10-S222TX, Gast Corp., USA) at 0.8 L min^{-1}. This instrumentation was housed in a sampling hut adjacent to the tower base (cf. Figure S2b). The testing of the profile system in the field and the QA/QC measurements are described in the Supporting Information (Section 1.1).

Data from the Hg^0 profile system were collected from August 2016 to March 2018. Overall, 6151 profiles were sampled, representing a data coverage of 57.7%. However, due to interruptions principally by power outages and instrumentation failures, the monthly coverage was unbalanced with >90% during February and August 2017 and January 2018 and <25% for November 2016, April 2017, and May 2017. The Hg^0 storage flux ($F_s^{Hg^0}$) is estimated as the difference between the vertical Hg^0 profiles $C(z,t)$ at the beginning and those at the end of the 80 min period T, divided by T following Finnigan (2006)[46]

$$F_s^{Hg^0} = \int_0^h \frac{1}{T}[C(z,\ T/2) - C(z,\ -T/2)]\mathrm{d}z \quad (1)$$

In addition, samples for Hg^0 isotopic composition determination were collected at the three levels z_1, z_6, and z_8 on chlorine-impregnated activated carbon (ClC, 1.0 g) traps at a volumetric flow rate of 6−8 L min^{-1} maintained by three lined pumps (model 72R655-V114-D304X, Gast Corp., USA). Isotopic Hg^0 profile samples were collected intermittently (April, September, October, and December during 2017), each for a 72−96 h period. The preconcentration procedure and mercury isotope analysis have been described elsewhere.[12]

https://doi.org/10.1021/acs.est.2c00778
Environ. Sci. Technol. 2022, 56, 5950−5959

Isotopic ratios were corrected for mass bias by an internal Tl standard (NIST SRM 997), and a standard-sample-standard bracketing method using NIST SRM 3133 was introduced for identifying Hg isotopic compositions. Following Blum and Bergquist,[47] our results were reported as δ^{xxx}Hg to describe mass-dependent fractionation and as Δ^{xxx}Hg to describe mass-independent fractionation.

$$\delta^{xxx}\mathrm{Hg}\ (‰) = \left[\left(\frac{^{xxx}\mathrm{Hg}}{^{198}\mathrm{Hg}}\right)_{\mathrm{sample}} \Big/ \left(\frac{^{xxx}\mathrm{Hg}}{^{198}\mathrm{Hg}}\right)_{\mathrm{NIST\ 3133}} - 1\right] \times 1000 \quad (2)$$

$$\Delta^{xxx}\mathrm{Hg} = \delta^{xxx}\mathrm{Hg} - \delta^{202}\mathrm{Hg} \times \beta_{xxx} \quad (3)$$

where *xxx* represents 199, 200, and 201, and β_{xxx} is 0.252 for ^{199}Hg, 0.502 for ^{200}Hg, and 0.752 for ^{201}Hg.

The results from QA/QC in isotope sampling and analysis are described in the Supporting Information (Section 1.2).

2.3. Above-Canopy Hg^0 Flux Measurements. A relaxed eddy accumulation (REA) system of the whole-air type with the design and operation parameters described elsewhere[48−50] was mounted on an instrumentation platform at 45 m above ground. Briefly, the REA apparatus (Figure S2a) consists of an open-path EC (OPEC) and a conditional gas sampling and analysis system. Tubings and fittings were subjected to dilute HCl (0.1 M) treatment, rinsed in Milli-Q water, and dried in a stream of zero air before being assembled. The OPEC part includes a 3D fast-response sonic anemometer (C-SAT3, Campbell Scientific) directed toward the prevailing wind direction and a micrologger with processing and control capabilities (CR5000, Campbell Scientific). Wind and temperature data collected at 10 Hz by the former were acquired and processed by the latter, which also control the execution of two fast-response conditional sampling valves (model 001-0017-900, Parker Fluidics, USA) following the implemented dynamic-wind dead-band algorithm ($w_{S'} > 0.3{\cdot}\sigma_w$, where σ_w and $w_{S'}$ are the standard deviation and absolute 5 min average of vertical wind in m s^{-1}, respectively) to accurately isolate up- and downdrafts present in sampled turbulent air parcels. Hg-free air (<0.1 ng m^{-3}) was supplied from a zero-air generator (Tekran model 1100) to the valves when sampling is not being conducted. Temporally synchronous Hg^0 concentration determination of the up- and downdraft channels[51,52] was achieved by using a Tekran model 1110 two-port sampling system synchronized with the 20-min sampling cycle of two Tekran model 2537X analyzers. Over a 40-min period (cycles I and II), the analyzers (denoted TK#1 and TK#2 below) determine the Hg^0 concentration in one updraft and one downdraft sample each, and the averaged turbulent flux ($F_{\mathrm{REA}}^{\mathrm{Hg}^0}$) is calculated according to

$$F_{\mathrm{REA}}^{\mathrm{Hg}^0} = \beta_T{\cdot}\sigma_w{\cdot}\Delta C_{\mathrm{REA}};\quad \Delta C_{\mathrm{REA}} = \underbrace{\frac{([C_{up}^{I}]^{TK\#1}+[C_{up}^{II}]^{TK\#2})/2}{C_{up}}} - \underbrace{\frac{([C_{dn}^{I}]^{TK\#1}+[C_{dn}^{II}]^{TK\#2})/2}{C_{dn}}} \quad (4)$$

where $[C_{up/dn}^{I/II}]^{TK\#1/TK\#2}$ is the Hg^0 concentration (at standard temperature and pressure) for the up- and downdraft samples, respectively, corrected for the dilution of zero-air injection[49] (ng m^{-3}). β_T is a dimensionless relaxation coefficient that was calculated for each averaging period (40 min) online from kinematic heat flux ($\overline{w'{\cdot}T'}$) measured by EC and synthesized from the REA algorithm

$$\beta_T = \overline{w'{\cdot}T'}/(\sigma_w{\cdot}[\overline{T_{up}} - \overline{T_{dn}}]) \quad (5)$$

where $\overline{T_{up}} - \overline{T_{dn}}$ is the difference between the sonic temperature in up- and downdrafts. If β_T deviated outside a ±0.2 interval of the median (most frequently during dawn, dusk, and night), the overall median value of 0.47 was implemented in eq 4.[53]

Using internal permeation source, the mercury analyzers were calibrated monthly or often more frequently due to power outage (calibrations within ±5% repeatability). The front filter of the REA intake line was replaced at the same interval. The leveling of the sonic anemometer was inspected biweekly. Hg^0 flux measurements were conducted during the period November 2016 to February 2018, with an overall data coverage of 63.1%. Gaps in the measurements were mainly attributed to power outages and instrumentation failures. To indicate periods of limited turbulent mixing that do not satisfy the requirement of MM theory,[54] data associated with a low friction velocity (u^* < 0.25 m s^{-1}) and/or high atmospheric stability (z/L > 1) were discarded resembling 11.2% of the total. Periods when horizontal wind approached outside the ±90° in-flow sector relative to the sonic anemometer head were also rejected to account for potential disturbances of the wind field (3.8% of the total). Spikes in flux data exceeding the range of monthly mean ± 3 SD were rejected.[36] Owing to the wind during ∼95% of the time derived from the large sector with uninterrupted forest for 2−3 km around the tower, the flux footprint of the REA measurement was consistently rendered to originate from the EB forest. After screening, a total of 7753 40-min Hg^0 flux data were included in the analyses described in the Results and Discussion section. The method detection limit (MDL) in ΔC_{REA} was determined to be ±0.045 ng m^{-3} (the procedure is described in the Supporting Information, Section 1.3 and Figure S3), and the proportion of Hg^0 flux data above the MDL was 51.2%. For data integration, however, we choose to apply the complete data set because average fluxes may otherwise be overestimated. Auxiliary equipment and corresponding measurement results important for our study are reported in the Supporting Information, Section 2.

3. RESULTS AND DISCUSSION

3.1. Concentrations and Isotopic Composition of Hg^0 in the Forest Ecosystem. During the 1.5-year sampling period between 2016 and 2018, the mean and median Hg^0 concentrations measured at ∼20 m above the EB forest canopy were 1.58 ± 0.65 and 1.37 ng m^{-3} (N = 6151), respectively. The mean concentration falls within the 1.3−1.6 ng m^{-3} annual mean period reported for background stations in the Northern Hemisphere.[55] Nevertheless, the data set displays a positive skewness driven by intermittent episodic Hg^0 peaks that are also shown in ground-based Hg^0 monitoring at ASSFERS (2 km distance) since 2011, which has been linked to long-range or transboundary transport of Hg^0 derived from, for example, industrial sources and biomass burning.[19,56] In our Hg^0 observations, episodical peaks above 4 ng m^{-3} occurred only from September to December and were associated with a monthly mean concentration range of 1.69−2.55 ng m^{-3}. Background Hg^0 concentrations prevailed during the period January to June 2017 (mean: 1.30−1.41 ng

https://doi.org/10.1021/acs.est.2c00778
Environ. Sci. Technol. 2022, 56, 5950−5959

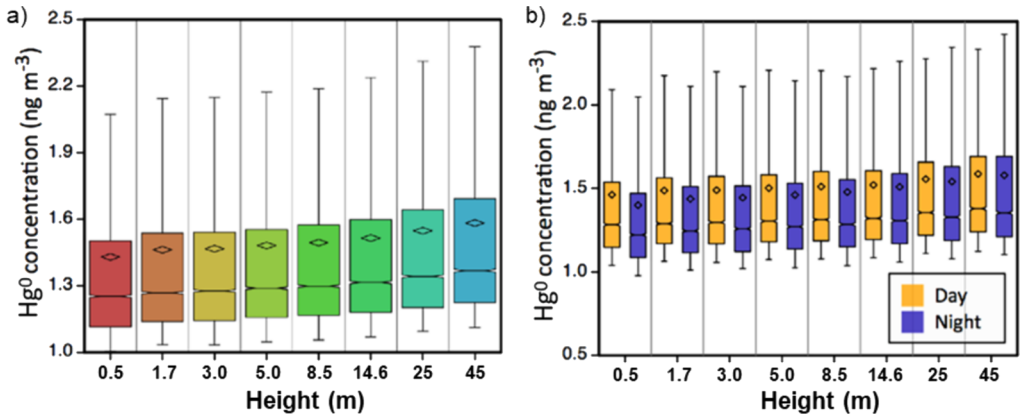

Figure 1. (a) Overall height segregated Hg^0 concentration observations. (b) Same data set split into day and night observations.

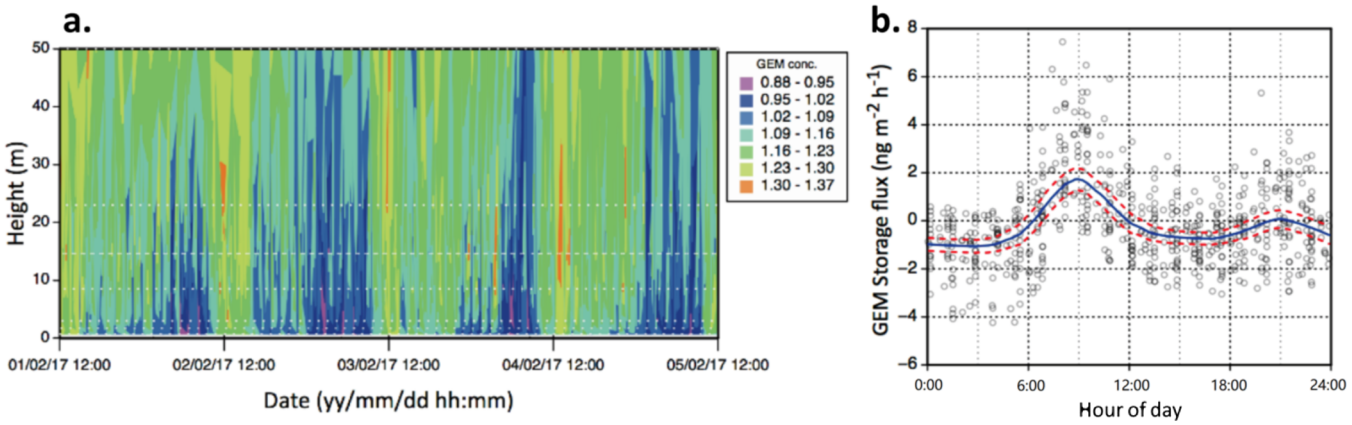

Figure 2. (a) Example of diurnal cycles observed in vertical Hg^0 concentrations for a couple of days associated with the lack of Hg^0 pollution events and relatively calm nights. (b) Diurnal variation in Hg^0 storage fluxes during the period January−March 2017, with a mean Hg^0 concentration range of 1.24 ± 0.17 ng m^{-3}. For exploratory reasons, the data were fitted with robust locally weighted regression (LOWESS) using a local smoothing width of 0.5.

m^{-3}). Hg^0 associated with the predominant wind directions of SSW—SE (70.2%) displays a lower mean concentration of 1.39 ± 0.37 ng m^{-3}, while a considerably higher (Welch's *t*-test, $p < 0.01$) Hg^0 mean concentration (2.30 ± 1.22 ng m^{-3}) occurred with infrequent northerlies (NNW—NNE, 7% of the time, Figure S5).

3.1.1. Vertical Distributions of Hg^0 Concentration and Storage Fluxes. The vertical distribution of Hg^0 concentrations during the study period is summarized in the box-and-whiskers plot of Figure 1a and Table S1. On average, the eight-level Hg^0 profile system showed a vertical gradient with significantly (Mann−Whitney U test, $p < 0.01$) increasing Hg^0 concentrations with each consecutive height above the ground level (a.g.l). The mean difference in Hg^0 concentrations between the highest (45 m a.g.l) and lowest (0.7 m a.g.l.) sampling level was 0.15 ± 0.09 ng m^{-3} [ΔC_{Hg^0} $(z_8 - z_1)$, n = 6155], accounting for ∼10% of the mean Hg^0 concentration at 45 m a.g.l. The mean in-canopy Hg^0 concentration difference [ΔC_{Hg^0} $(z_7 - z_1)$] was 0.12 ± 0.07 ng m^{-3}, which demonstrates that the forest canopy acts as a net sink for atmospheric Hg^0. Moreover, the lowest in-canopy mean Hg^0 concentration (1.43 ± 0.59 ng m^{-3}) was observed at the height closest to the forest floor, which was on average 0.026 ± 0.015 ng m^{-3} lower (Mann−Whitney *U* test, $p < 0.01$) than that at 1.7 m a.g.l., implying a significant Hg^0 removal process at or near the forest floor. Although the mean Hg^0 concentration at 45 m between day (06:40−18:30) and night (18:40−06:30) differed insignificantly (1.59 ± 0.62 and 1.58 ± 0.67 ng m^{-3}, respectively; Student's *t*-test, $p > 0.10$), the mean ΔC_{Hg^0} $(z_7 - z_1)$ became more extensive during the night (0.14 ± 0.08 ng m^{-3}) than during the day (0.10 ± 0.06 ng m^{-3}). During the night, the relative contribution of the lower canopy ($z \leq z_6$) to the Hg^0 gradient increased substantially (Table S1 and Figure 1b), which may stem from occasional nocturnal decoupling of airspaces within and above the canopy.[54] The typical daily cycle of increased vertical mixing during the daytime will mitigate in-canopy gradients. However, concerning the lower canopy below the layer of the highest leaf area density ($z < 8$ m), the measured turbulence profile [$\sigma_w(z)/u^*$, Figure S1] indicates that the vertical mixing of air is limited over the diel cycle.

Figure 2a shows an example of diurnal cycles observed in vertical Hg^0 concentrations for a couple of days, which is associated with the lack of Hg^0 pollution events and relatively calm nights. A decrease in foremost understory Hg^0 in the evening followed by partial Hg^0 depletion at night and rapid Hg^0 buildup after sunrise are clearly shown. Figure 2 corresponds to a predominantly negative Hg^0 storage flux at night and a larger magnitude of positive storage occurring during early morning hours. Associated with Hg^0 pollution plumes, the magnitude of the Hg^0 storage flux calculated by eq 1 becomes large (typically >20 ng m^{-2} h^{-1}). Although the

https://doi.org/10.1021/acs.est.2c00778
Environ. Sci. Technol. 2022, 56, 5950−5959

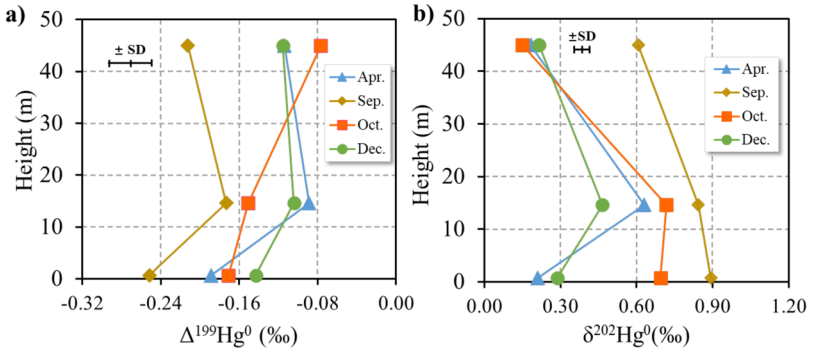

Figure 3. Vertical profiles of $\Delta^{199}Hg^0$ (a) and $\delta^{202}Hg^0$ (b) in and above the forest collected during 72−96 h for each of the indicated months (for details, cf. Table S2).

mean over such events (and longer periods, such as a month) theoretically should be near zero,[41] we observe with our 80 min minimum resolution capability that averages for months characterized by pollution deviated considerably from zero. Therefore, we assess that the time resolution for the gradient measurements is too poor to correctly construct the diurnal variation of Hg-NEE ($F_{REA}^{Hg^0} + F_s^{Hg^0}$) over the seasons during a year. Figure 2b shows the daily variation in storage fluxes for limited periods of time with low Hg^0 variability ($\sigma \leq 0.3$ ng m^{-3}) and daily mean values of storage near zero. Monthly mean night-time F_s fell in the range of −0.4 to −1.1 ng m^{-2} h^{-1}, while for the time interval of 07:00−10:00 surrounding the morning peak in F_s, monthly mean values were in the range 1.8−2.5 ng m^{-2} h^{-1}. In future work, a much shorter time window to resolve a Hg^0 profile possible with a shift in instrumentation is required to properly target periods of considerable concentration change.[1]

3.1.2. Vertical Profiles of Hg^0 Isotope Composition in Air. The isotopic composition of Hg^0 observations (Table S2) at the ASSFERS eddy tower displays moderately negative $\Delta^{199}Hg^0$ (from −0.25 to −0.08‰) and more pronounced positive $\delta^{202}Hg^0$ (from 0.15 to 0.89‰), which is characteristic of forested[6,12,40,57] and other remote vegetated[37,58,59] ecosystems. As shown in Figure 3b, there is a continuous difference in $\delta^{202}Hg^0$ values between level z_6 and z_8 (mean: 0.38 ± 0.16‰), with a significantly higher (paired t-test, $p < 0.01$) $\delta^{202}Hg^0$ in the air within the canopy compared with above the canopy. Such enrichment of heavy Hg^0 isotopes in the canopy air is consistent with the preferential uptake of lighter Hg^0 isotopes by vegetation.[12] The aforementioned trend in $\delta^{202}Hg^0$ also occurred in the air near the forest floor (z_1) during the rainy season compared with the air at 45 m (mean difference: 0.38‰), but taking into account observations during the dry season, the overall difference was insignificant (paired t-test, $p > 0.10$). For $\Delta^{199}Hg^0$, the lowest part of the canopy presents a moderately significant (paired t-test, $p < 0.05$) difference compared with above the canopy as well as with the upper canopy (Figure 3a). More negative $\Delta^{199}Hg^0$ and $\delta^{202}Hg^0$ values measured in the air near the forest floor are consistent with observations from the adjacent air−soil flux chamber measurements and probing of Hg^0 in the soil pore air with distinct negative signatures.[60] The largest gradient in both $\delta^{202}Hg^0$ (0.39‰) and $\Delta^{199}Hg^0$ (0.10‰) was observed during April, when the mid-height attained the most positive values. The $\delta^{202}Hg^0$ in modified air (deficit in Hg^0 by foliar uptake) was linearly correlated with the magnitude of the Hg^0 uptake.[12] Interestingly, there is a positive correlation between $\Delta^{199}Hg^0$ and the Hg^0 net uptake flux, highlighting the bidirectional exchange associated with foliar surfaces.[12] The foliage re-emission flux is isotopically distinct and contributes to a more positive $\Delta^{199}Hg^0$ signature in the surrounding air. It should be clarified that $\Delta^{199}Hg^0$ is shifted overall to more positive values when ASSFERS receives polluted air.[57] In addition to the April observation, the profile from September shows a local $\Delta^{199}Hg^0$ maximum in the upper canopy, suggesting that Hg^0 re-emission competes to a substantial degree with foliar uptake. Both being temperate months, April represents the end of the dry season with a high number of sunshine hours, while September is warmer, with sporadic rain and sunshine.[33]

3.2. Air−Forest Hg^0 Exchange Fluxes. Hg^0 flux data at a 40-min temporal resolution and the cumulative Hg^0 flux over the study period are presented in Figure 4 with selected meteorological parameters. Bidirectional Hg^0 fluxes displayed a large temporal variability ranging from −501.3 to 461.9 ng m^{-2} h^{-1}, which is comparable to previous Hg^0 flux measurements conducted over forests by MM techniques.[34−36] A Shapiro−Wilk's test indicated that the distribution of flux data was not significantly different from a normal distribution ($p > 0.10$), and in the following analysis, mean and standard deviation were used as data descriptors. The Hg^0 flux measurement above the canopy shows that the EB forest acts as a year-round sink of atmospheric Hg^0 with a cumulative flux of −41.1 μg m^{-2} based on the entire screened raw data set (Figure 4). The corresponding mean Hg^0 flux was −7.8 ng m^{-2} h^{-1} ($n = 7753$), with most Hg^0 dry deposition (86% of total cumulative flux) occurring at the end of the wet season (September−October) and during the cold and dry subseason (November−February). In contrast, a weaker net Hg^0 deposition was observed during the mild and dry subseason (March−May), coinciding with the period of lowest annual NVDI.[40] Altitude-induced low temperature and cloudiness are two main factors that contribute to ASSFERS being a major carbon sink.[33] Although Hg^0 flux data nominally show 63.1% coverage, these data are unbalanced among months with relatively low coverage (principally due to power outages) especially from May to July (25−36% coverage, Table 1). To construct a net annual Hg^0 flux estimate, we computed the monthly averages and diel courses as tools to fill in data gaps. During the periods that are mostly characterized by a relatively low light and moist conditions (October−February), the diel variation shows a relatively monotonous dry deposition that is greatest in the afternoon (Figure 5b). In spring, there is a shift in the pattern that can be explained by stronger light-driven re-emissions that counterbalance the reverse-directed foliar Hg^0 uptake during

https://doi.org/10.1021/acs.est.2c00778
Environ. Sci. Technol. 2022, 56, 5950−5959

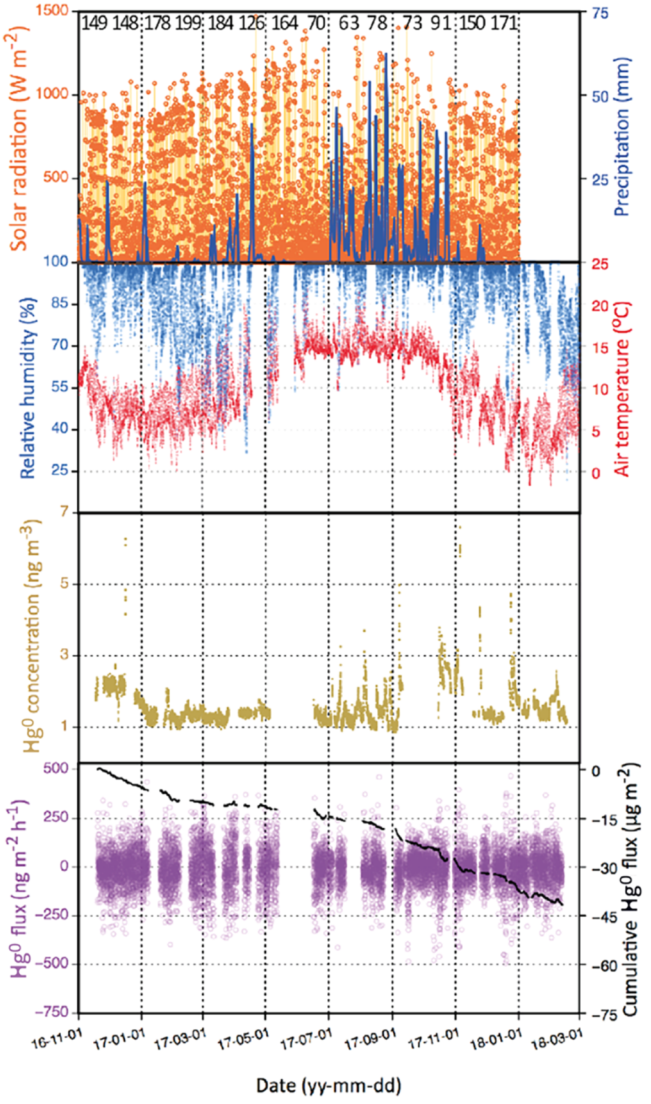

Figure 4. Time series of the selected above canopy measurement data from the ASSFERS eddy tower. Panels from the top downward: (1) sunshine hours per month, left: global radiation (W m^{-2}, orange line with mounted circle) and right: event precipitation (mm, blue line); (2) left: relative humidity (%, blue dots) and right: air temperature (°C, red dots); (3) Hg^0 concentration (ng m^{-3}, golden dots) and (4) left: Hg^0 flux (ng m^{-3}, purple dots) and right: cumulative Hg^0 flux (μg m^{-2}, black dots).

the day (Figure 5a), a flux partitioning that is supported by the isotope measurements. The estimated monthly averages (Table 1) were summed up to yield an annual Hg^0 flux in the range of -53.9 ± 19.8 μg m^{-2}. The stated uncertainty was calculated by standard error propagation of the variances in the monthly averages, which was derived by a 24 h differencing approach.[41] Based on overlapping measurements for December and January over two calendar years, the interannual variation amounts to less than 20%, which is less than the uncertainty in the annual exchange of atmospheric Hg^0 with the evergreen broadleaf forest ecosystem. Further details on the QA/QC assessment for estimating uncertainties and systematic errors are given in the Supporting Information, Section 1.

Although the gradient and REA flux measurements and the eddy tower instrumentation for meteorological monitoring

Table 1. Estimated Monthly Hg^0 Fluxes and Associated Uncertainties

month	estimated cumulative Hg^0 flux (μg m^{-2})[a]	uncertainty (1σ)	data coverage (%)
January	−6.8	1.2	75.3
February	−5.0	1.4	69.2
March	−1.4	1.6	61.0
April	−1.0	0.8	47.8
May	−1.6	1.0	25.4
June	−2.8	1.3	36.4
July	−3.2	1.1	36.2
August	−4.4	1.2	65.7
September	−6.3	1.0	87.1
October	−7.3	1.1	86.3
November	−6.9	1.3	75.6
December	−7.2	1.0	91.3
total	−53.9	19.8	63.1

[a]Derived by gap filling, where each missing data entry was replaced by the value predicted by the smoothed diurnal features (depicted in Figure 5) for the current day and month.

were not completely synchronized, branch-level fluxes partially contemporary with the above canopy observations show correlations with PAR and air temperature and anticorrelations with relative humidity and air Hg^0 concentration.[12] It should be noted that REA and chamber techniques are based on different physical principles. The enclosure method is subject to microenvironment conditions that are significantly perturbed from the ambient foremost by solar heating,[61] which may underscore any relationship between flux and controlling parameters. Such an interior greenhouse effect may explain why the chamber measurements indicate a forest-floor annual Hg^0 net source (6.7 ± 20.5 μg m^{-2} yr^{-1})[62] that is contradictory to prevailing negative Hg^0 concentration profiles in-canopy toward the ground (Figure S6).

3.3. Discussion. Fluxes measured by micrometeorological methods estimated the net sum of the Hg^0 source and sink terms in the ecosystem in exchange for the atmosphere. There are distinct correspondences between the diel features of the whole-ecosystem Hg^0 flux over evergreen canopies and those previously reported over mid-latitudinal deciduous canopies.[4,30,35] For example, the pattern coincides during the peak vegetation season (Figure 5b)[34,35,63,64] and during the spring with the lowest NVDI at ASSFERS and mid-latitudinal forests in vegetation (Figure 5a).[35] Based on branch-level measurements for a selection of the most common tree species in ASSFERS, we previously attempted a bottom-up quantification of annual Hg^0 air-leaf gas exchange yielding -26.8 ± 12.7 μg m^{-2}.[12] However, data were limited in both time and space, where these branch-level fluxes represent the lowest part of the foliage during weekly campaigns distributed among seasons. Species-specific trends in aboveground foliar Hg^0 fluxes have been identified depending on leaf placement, age, and crown height.[65−67] Unaccounted for in our bottom-up quantification, leaves at the top of the crown (sun leaves) possess, for beech, Hg^0 uptake fluxes that can be more than twice as large as those for shaded leaves further down.[67] Disregarding the interaction with fan bryophytes and liana, and other aboveground woody biomass, in-canopy Hg^0 sinks approximated through the bottom-up approach were underestimated and should be regarded as a lower limit of the net sink.[9,29] Additionally, with the advent of analyses of stable Hg

https://doi.org/10.1021/acs.est.2c00778
Environ. Sci. Technol. 2022, 56, 5950−5959

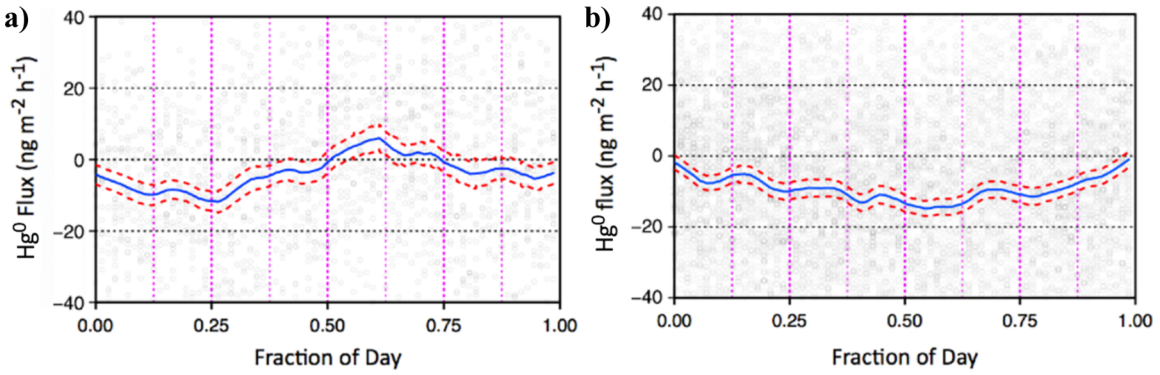

Figure 5. LOWESS-smoothed diurnal features of Hg^0 flux. (a) Data from March to May and (b) data from October to February. The line and envelope depict the mean and $\pm 1\sigma$, respectively.

isotopes, it is becoming increasingly evident that atmospherically sourced Hg^0 participates not only in dry deposition/uptake but also considerably in hydrological processes occurring in the canopy.[9,68] Interestingly, Hg in throughfall differs isotopically from that in wet deposition by significant negative shifts in $\delta^{202}Hg$, $\Delta^{199}Hg$, and $\Delta^{200}Hg$, which is consistent with mercury previously taken up as Hg^0 going into the solution when the substrate is wetted by precipitation rich in DOC.[9] Therefore, caution is warranted when scaling up Hg^0 fluxes measured with chambers to be representative of a large area. Interestingly, the common indirect method involving the sum of litterfall and throughfall minus bulk wet deposition as a proxy for total Hg dry deposition[69] and litterfall deposition as a proxy for Hg^0 dry deposition[70] also produces a substantial underestimation. The indirect approach gives an annual total Hg dry deposition of 54.9 ± 11.2 $\mu g\ m^{-2}\ yr^{-1}$,[42] which differs insignificantly from the annual estimate of Hg^0 deposition by the REA technique (53.9 $\mu g\ m^{-2}\ yr^{-1}$). The latter quantity preliminarily in turn exceeds the litterfall Hg input by 80%, while diverging results are reported for deciduous hardwood forests in New England (−55[34] and 200%,[35] respectively). Consequently, our observations clearly mark what Obrist et al.[35] previously articulated, namely, that the frequent application of Hg in litterfall as a proxy[70,71] for whole-ecosystem net deposition of Hg^0 is severely flawed.

Considering the forest Hg^0 flux database compiled in the literature,[2,3] our estimate belongs to the lowest (most negative) quartile of fluxes. The finding that an intact primary subtropical forest is a strong sink for atmospheric Hg^0 is not surprising.[4] However, the observed sink in this study indicates that the sink term is significantly greater than what has been observed elsewhere (Table S3). Similar to mature forests being an important CO_2 sink, the undisturbed Fagaceae forest of ASSFERS displays a large absolute CO_2 NEE (−0.7 to −0.9 kg $m^{-2}\ yr^{-1}$),[33,44] because CO_2 and Hg^0 sequestration is closely connected through foliar stomatal processes.[10,35,65] Most foliar Hg^0 uptake occurs in older secondary natural and seminatural forests and less in plantation and young forest regrowth.[72] Nevertheless, species-specific differences exist between foliar Hg concentrations present in softwood and deciduous hardwood forests.[73] Recently, Wohlgemuth et al. have quantified substantially higher foliar net Hg^0 uptake for deciduous broadleaf species of the *Fagaceae* family (up to 26 $\mu g\ m^{-2}$) compared with pine (4 ± 1 $\mu g\ m^{-2}$) in a survey of a latitudinal transect across Europe.[67] By sampling along a forest chronosequence at a deglaciated terrain of SW China, it was found that atmospheric Hg^0 was the predominant source (75−90%) of Hg in woody biomass (bole wood and bark) and cryptogamic covers.[9] For hardwood, the Hg pool in aboveground woody biomass may exceed that in foliage per land area unit.[27] However, the size of the Hg pool of moss biomass and necromass in an old-growth primary forest plausibly exceeds that in both foliage and tree wood.[9,26] Our Hg^0 flux measurements indicate that plant tissue other than the foliage makes a significant contribution to the observed Hg^0 deposition. Analogous to previous studies,[14,35] the gradient measurements below the canopy (Supporting Information, Section 3) also suggest that the forest floor is an overall net sink for Hg^0 (Figure S6).

4. Implications. In the context of previous flux studies in China's forest ecosystems (reviewed in Zhou et al.,[74] cf. Table S3), our results agree that atmospheric Hg dry deposition is generally high (>80% of an average total Hg deposition of 73.9 $\mu g\ m^{-2}\ yr^{-1}$).[4,35] In terms of the role of atmospheric Hg^0 as an ecosystem source or sink, the results differ from the findings of other studies that consider air-foliage Hg^0 exchange in subtropical China.[36,71,75] Investigations by micrometeorological techniques show that two reclaimed, relatively young (~30 yr) and atmospherically impacted (mean Hg^0 concentrations of 3.6 and 5.9 ng m^{-3}) coniferous plantations act as Hg^0 net sources of divergent strength (Masson pine 58.5 and Chinese fir 2.7 $\mu g\ m^{-2}$). The only other long-term study by a micrometeorological technique of a vegetated ecosystem under anthropogenic influence in China, namely, a cereal cropland in the North China Plain (NCP), also shows that it is a net source of Hg^0 summed over an entire year.[48] In this case, the high dry deposition in NCP propels a general dominance of soil emissions during daytime in relation to Hg^0 uptake by overlying foliage regardless of canopy cover. Even though the average value of the reported forest floor net emissions is very high in the Masson pine stand (47.6 $\mu g\ m^{-2}\ yr^{-1}$),[71] the perennial needles give an annual net addition of atmospheric Hg^0.[36,75] With an estimated Hg^{II} dry deposition of 64−70 $\mu g\ m^{-2}$ at sites in central southern China, Yu et al.[71] argued that recently falling Hg^{II} inputs and Hg^0 concentrations promote subtropical forest Hg^0 emissions. This far-reaching assumption is not supported by the present study of a protected subtropical forest and may, in our opinion, need more elaboration by the study of a larger and more representative set of forest ecosystems and by the inclusion of isotope studies to ascertain Hg^0 sinks. We predict that the investigated ecosystem located in a protected area will remain a large Hg^0 sink, but that an increased frequency of extreme weather due to climate change (e.g., drought, icestorms) introduces damage to

https://doi.org/10.1021/acs.est.2c00778
Environ. Sci. Technol. 2022, 56, 5950−5959

the ecosystem that can take several years to recover.[76] Nevertheless, on-going afforestation and vegetation restoration in degraded ecosystems of mainland China have the long-term effect that an increasing amount of Hg^0 is regionally removed from the atmosphere.[77] However, from a global perspective, anthropogenic effects through land use and climate change—induced processes such as permafrost thaw, drought, wildfires and deforestation in the tropics appear to critically increase the net supply of Hg to the atmosphere.[1] Such a scenario in the Anthropocene entails that more Hg is mobilized into relatively fast flux cycles through which it becomes more dispersed and available, for example, various processes yielding organic Hg with elevated toxicity for humankind.[78]

■ ASSOCIATED CONTENT

Supporting Information

The Supporting Information is available free of charge at https://pubs.acs.org/doi/10.1021/acs.est.2c00778.

Vertical Hg^0 concentration profile, isotopic composition of Hg^0 in air, summary of previous forest Hg^0 flux studies, vertical profiles of turbulence and LAI, schematics of the MM Hg^0 flux instrumentation, corresponding QA/QC assessment , plot of basic meteorological parameters, polar plot showing the distribution of airborne Hg^0 concentration with the wind direction, and temporal plot of vertical profile layer Hg^0 concentration differences (PDF)

The time series of data that support the findings of this study is available upon request.

■ AUTHOR INFORMATION

Corresponding Authors

Xinbin Feng − *State Key Laboratory of Environmental Geochemistry, Institute of Geochemistry, Chinese Academy of Sciences, Guiyang 550081, China; Center for Excellence in Quaternary Science and Global Change, Chinese Academy of Sciences, Xian 710061, China;* orcid.org/0000-0002-7462-8998; Phone: +86-851-85895728; Email: fengxinbin@vip.skleg.cn; Fax: +86-851-5891609

Jonas Sommar − *State Key Laboratory of Environmental Geochemistry, Institute of Geochemistry, Chinese Academy of Sciences, Guiyang 550081, China;* orcid.org/0000-0001-8634-440X; Phone: +86-18275032610; Email: jonas@vip.skleg.cn

Authors

Bo Wang − *State Key Laboratory of Environmental Geochemistry, Institute of Geochemistry, Chinese Academy of Sciences, Guiyang 550081, China; University of Chinese Academy of Sciences, Beijing 100049, China*

Wei Yuan − *State Key Laboratory of Environmental Geochemistry, Institute of Geochemistry, Chinese Academy of Sciences, Guiyang 550081, China*

Xun Wang − *State Key Laboratory of Environmental Geochemistry, Institute of Geochemistry, Chinese Academy of Sciences, Guiyang 550081, China;* orcid.org/0000-0002-7407-8965

Kai Li − *State Key Laboratory of Environmental Geochemistry, Institute of Geochemistry, Chinese Academy of Sciences, Guiyang 550081, China*

Che-Jen Lin − *Center for Advances in Water and Air Quality, Lamar University, Beaumont, Texas 77710, United States*

Ping Li − *State Key Laboratory of Environmental Geochemistry, Institute of Geochemistry, Chinese Academy of Sciences, Guiyang 550081, China; Center for Excellence in Quaternary Science and Global Change, Chinese Academy of Sciences, Xian 710061, China;* orcid.org/0000-0002-0145-4122

Zhiyun Lu − *National Forest Ecosystem Research Station at Ailaoshan, Jingdong, Yunnan 676209, China*

Complete contact information is available at: https://pubs.acs.org/10.1021/acs.est.2c00778

Funding

This work was funded by the National Natural Science Foundation of China (grants 41829701, 41921004, and 42007307).

Notes

The authors declare no competing financial interest.

■ REFERENCES

(1) Sommar, J.; Osterwalder, S.; Zhu, W. Recent advances in understanding and measurement of Hg in the environment: Surface-atmosphere exchange of gaseous elemental mercury (Hg-0). *Sci. Total Environ.* **2020**, *721*, 137648.

(2) Agnan, Y.; Le Dantec, T.; Moore, C. W.; Edwards, G. C.; Obrist, D. New constraints on terrestrial surface-atmosphere fluxes of gaseous elemental mercury using a global database. *Environ. Sci. Technol.* **2016**, *50*, 507−524.

(3) Zhu, W.; Lin, C.-J.; Wang, X.; Sommar, J.; Fu, X.; Feng, X. Global observations and modeling of atmosphere-surface exchange of elemental mercury: a critical review. *Atmos. Chem. Phys.* **2016**, *16*, 4451−4480.

(4) Zhou, J.; Obrist, D.; Dastoor, A.; Jiskra, M.; Ryjkov, A. Vegetation uptake of mercury and impacts on global cycling. *Nat. Rev. Earth Environ.* **2021**, *2*, 269−284.

(5) Lyman, S. N.; Cheng, I.; Gratz, L. E.; Weiss-Penzias, P.; Zhang, L. An updated review of atmospheric mercury. *Sci. Total Environ.* **2020**, *707*, 135575.

(6) Demers, J. D.; Blum, J. D.; Zak, D. R. Mercury isotopes in a forested ecosystem: Implications for air-surface exchange dynamics and the global mercury cycle. *Global Biogeochem. Cycles* **2013**, *27*, 222−238.

(7) Enrico, M.; Roux, G. L.; Marusczak, N.; Heimbürger, L.-E.; Claustres, A.; Fu, X.; Sun, R.; Sonke, J. E. Atmospheric Mercury Transfer to Peat Bogs Dominated by Gaseous Elemental Mercury Dry Deposition. *Environ. Sci. Technol.* **2016**, *50*, 2405−2412.

(8) Obrist, D.; Agnan, Y.; Jiskra, M.; Olson, C. L.; Colegrove, D. P.; Hueber, J.; Moore, C. W.; Sonke, J. E.; Helmig, D. Tundra uptake of atmospheric elemental mercury drives Arctic mercury pollution. *Nature* **2017**, *547*, 201−204.

(9) Wang, X.; Yuan, W.; Lin, C.-J.; Luo, J.; Wang, F.; Feng, X.; Fu, X.; Liu, C. Underestimated Sink of Atmospheric Mercury in a Deglaciated Forest Chronosequence. *Environ. Sci. Technol.* **2020**, *54*, 8083−8093.

(10) Jiskra, M.; Sonke, J. E.; Obrist, D.; Bieser, J.; Ebinghaus, R.; Myhre, C. L.; Pfaffhuber, K. A.; Wängberg, I.; Kyllönen, K.; Worthy, D.; Martin, L. G.; Labuschagne, C.; Mkololo, T.; Ramonet, M.; Magand, O.; Dommergue, A. A vegetation control on seasonal variations in global atmospheric mercury concentrations. *Nat. Geosci.* **2018**, *11*, 244−250.

(11) Bash, J. O.; Bresnahan, P.; Miller, D. R. Dynamic surface interface exchanges of mercury: A review and compartmentalized modeling framework. *J. Appl. Meteorol. Climatol.* **2007**, *46*, 1606−1618.

(12) Yuan, W.; Sommar, J.; Lin, C.-J.; Wang, X.; Li, K.; Liu, Y.; Zhang, H.; Lu, Z.; Wu, C.; Feng, X. Stable Isotope Evidence Shows Re-emission of Elemental Mercury Vapor Occurring after Reductive Loss from Foliage. *Environ. Sci. Technol.* **2019**, *53*, 651−660.

(13) Wang, X.; Bao, Z.; Lin, C.-J.; Yuan, W.; Feng, X. Assessment of Global Mercury Deposition through Litterfall. *Environ. Sci. Technol.* **2016**, *50*, 8548−8557.
(14) Fu, X.; Zhu, W.; Zhang, H.; Sommar, J.; Yu, B.; Yang, X.; Wang, X.; Lin, C.-J.; Feng, X. Depletion of atmospheric gaseous elemental mercury by plant uptake at Mt. Changbai, Northeast China. *Atmos. Chem. Phys.* **2016**, *16*, 12861−12873.
(15) Ma, M.; Du, H.; Wang, D. A New Perspective is Required to Understand the Role of Forest Ecosystems in Global Mercury Cycle: A Review. *Bull. Environ. Contam. Toxicol.* **2019**, *102*, 650.
(16) Wang, Z.; Zhang, X.; Xiao, J.; Zhijia, C.; Yu, P. Mercury fluxes and pools in three subtropical forested catchments, southwest China. *Environ. Pollut.* **2009**, *157*, 801−808.
(17) Zhou, J.; Feng, X.; Liu, H.; Zhang, H.; Fu, X.; Bao, Z.; Wang, X.; Zhang, Y. Examination of total mercury inputs by precipitation and litterfall in a remote upland forest of Southwestern China. *Atmos. Environ.* **2013**, *81*, 364−372.
(18) Wang, X.; Lin, C.-J.; Lu, Z.; Zhang, H.; Zhang, Y.; Feng, X. Enhanced accumulation and storage of mercury on subtropical evergreen forest floor: Implications on mercury budget in global forest ecosystems. *J. Geophys. Res.: Biogeosci.* **2016**, *121*, 2096−2109.
(19) Zhang, H.; Fu, X.; Lin, C.-J.; Shang, L.; Zhang, Y.; Feng, X.; Lin, C. Monsoon-facilitated characteristics and transport of atmospheric mercury at a high-altitude background site in southwestern China. *Atmos. Chem. Phys.* **2016**, *16*, 13131−13148.
(20) Lu, Z.; Wang, X.; Zhang, Y.; Zhang, Y.-J.; Luo, K.; Sha, L. High mercury accumulation in two subtropical evergreen forests in South China and potential determinants. *J. Environ. Manage.* **2016**, *183*, 488−496.
(21) Poissant, L.; Pilote, M.; Yumvihoze, E.; Lean, D. Mercury concentrations and foliage/atmosphere fluxes in a maple forest ecosystem in Quebec, Canada. *J. Geophys. Res.: Atmos.* **2008**, *113*, D10307.
(22) Graydon, J. A.; St Louis, V. L.; Lindberg, S. E.; Hintelmann, H.; Krabbenhoft, D. P. Investigation of mercury exchange between forest canopy vegetation and the atmosphere using a new dynamic chamber. *Environ. Sci. Technol.* **2006**, *40*, 4680−4688.
(23) Millhollen, A. G.; Gustin, M. S.; Obrist, D. Foliar mercury accumulation and exchange for three tree species. *Environ. Sci. Technol.* **2006**, *40*, 6001−6006.
(24) Karl, T.; Potosnak, M.; Guenther, A.; Clark, D.; Walker, J.; Herrick, J. D.; Geron, C. Exchange processes of volatile organic compounds above a tropical rain forest: Implications for modeling tropospheric chemistry above dense vegetation. *J. Geophys. Res.: Atmos.* **2004**, *109*, D18306.
(25) Arnold, J.; Gustin, M. S.; Weisberg, P. J. Evidence for Nonstomatal Uptake of Hg by Aspen and Translocation of Hg from Foliage to Tree Rings in Austrian Pine. *Environ. Sci. Technol.* **2018**, *52*, 1174−1182.
(26) Liu, H.-w.; Shao, J.-j.; Yu, B.; Liang, Y.; Duo, B.; Fu, J.-j.; Yang, R.-q.; Shi, J.-b.; Jiang, G.-b. Mercury isotopic compositions of mosses, conifer needles, and surface soils: Implications for mercury distribution and sources in Shergyla Mountain, Tibetan Plateau. *Ecotoxicol. Environ. Saf.* **2019**, *172*, 225−231.
(27) Yang, Y.; Yanai, R. D.; Driscoll, C. T.; Montesdeoca, M.; Smith, K. T. Concentrations and content of mercury in bark, wood, and leaves in hardwoods and conifers in four forested sites in the northeastern USA. *PLoS One* **2018**, *13*, No. e0196293.
(28) Harmens, H.; Norris, D. A.; Koerber, G. R.; Buse, A.; Steinnes, E.; Rühling, Å. Temporal trends (1990-2000) in the concentration of cadmium, lead and mercury in mosses across Europe. *Environ. Pollut.* **2008**, *151*, 368−376.
(29) Liu, Y.; Lin, C.-J.; Yuan, W.; Lu, Z.; Feng, X. Translocation and distribution of mercury in biomasses from subtropical forest ecosystems: evidence from stable mercury isotopes. *Acta Geochim.* **2021**, *40*, 42−50.
(30) Wang, X.; Yuan, W.; Lin, C.-J.; Feng, X. Mercury cycling and isotopic fractionation in global forests. *Crit. Rev. Environ. Sci. Technol.* **2021**, *52*, 1−24.
(31) Wang, X.; Luo, J.; Yuan, W.; Lin, C.-J.; Wang, F.; Liu, C.; Wang, G.; Feng, X. Global warming accelerates uptake of atmospheric mercury in regions experiencing glacier retreat. *Proc. Natl. Acad. Sci. U.S.A.* **2020**, *117*, 2049−2055.
(32) Tan, Z.-H.; Zhang, Y.-P.; Liang, N.; Hsia, Y.-J.; Zhang, Y.-J.; Zhou, G.-Y.; Li, Y.-L.; Juang, J.-Y.; Chu, H.-S.; Yan, J.-H.; Yu, G.-R.; Sun, X.-M.; Song, Q.-H.; Cao, K.-F.; Schaefer, D. A.; Liu, Y.-H. An observational study of the carbon-sink strength of East Asian subtropical evergreen forests. *Environ. Res. Lett.* **2012**, *7*, 044017.
(33) Tan, Z.-H.; Zhang, Y.-P.; Schaefer, D.; Yu, G.-R.; Liang, N.; Song, Q.-H. An old-growth subtropical Asian evergreen forest as a large carbon sink. *Atmos. Environ.* **2011**, *45*, 1548−1554.
(34) Bash, J. O.; Miller, D. R. Growing season total gaseous mercury (TGM) flux measurements over an Acer rubrum L. stand. *Atmos. Environ.* **2009**, *43*, 5953−5961.
(35) Obrist, D.; Roy, E. M.; Harrison, J. L.; Kwong, C. F.; Munger, J. W.; Moosmüller, H.; Romero, C. D.; Sun, S.; Zhou, J.; Commane, R. Previously unaccounted atmospheric mercury deposition in a midlatitude deciduous forest. *Proc. Natl. Acad. Sci. U.S.A.* **2021**, *118*, No. e2105477118.
(36) Yu, Q.; Luo, Y.; Wang, S.; Wang, Z.; Hao, J.; Duan, L. Gaseous elemental mercury (GEM) fluxes over canopy of two typical subtropical forests in south China. *Atmos. Chem. Phys.* **2018**, *18*, 495−509.
(37) Jiskra, M.; Sonke, J. E.; Agnan, Y.; Helmig, D.; Obrist, D. Insights from mercury stable isotopes on terrestrial−atmosphere exchange of Hg(0) in the Arctic tundra. *Biogeosciences* **2019**, *16*, 4051−4064.
(38) Lan, X.; Talbot, R.; Castro, M.; Perry, K.; Luke, W. Seasonal and diurnal variations of atmospheric mercury across the US determined from AMNet monitoring data. *Atmos. Chem. Phys.* **2012**, *12*, 10569−10582.
(39) Mao, H.; Talbot, R. W.; Sigler, J. M.; Sive, B. C.; Hegarty, J. D. Seasonal and diurnal variations of Hg^0 over New England. *Atmos. Chem. Phys.* **2008**, *8*, 1403−1421.
(40) Fu, X.; Zhang, H.; Liu, C.; Zhang, H.; Lin, C.-J.; Feng, X. Significant Seasonal Variations in Isotopic Composition of Atmospheric Total Gaseous Mercury at Forest Sites in China Caused by Vegetation and Mercury Sources. *Environ. Sci. Technol.* **2019**, *53*, 13748−13756.
(41) Aubinet, M.; Vesala, T.; Papale, D. *Eddy Covariance*; Springer Verlag, 2012.
(42) Feng, X. Stable isotope fractionation induced from mercury biogeochemical cycling in a subtropical evergreen forest ecosystem. In *14th International Conference on Mercury as a Global Pollutant*: Kraków, Poland, 2019.
(43) Liu, W.; Fox, J. E. D.; Xu, Z. Nutrient budget of a montane evergreen broad-leaved forest at Ailao Mountain National Nature Reserve, Yunnan, southwest China. *Hydrol. Process.* **2003**, *17*, 1119−1134.
(44) Fei, X.; Song, Q.; Zhang, Y.; Liu, Y.; Sha, L.; Yu, G.; Zhang, L.; Duan, C.; Deng, Y.; Wu, C.; Lu, Z.; Luo, K.; Chen, A.; Xu, K.; Liu, W.; Huang, H.; Jin, Y.; Zhou, R.; Li, J.; Lin, Y.; Zhou, L.; Fu, Y.; Bai, X.; Tang, X.; Gao, J.; Zhou, W.; Grace, J. Carbon exchanges and their responses to temperature and precipitation in forest ecosystems in Yunnan, Southwest China. *Sci. Total Environ.* **2018**, *616*−*617*, 824−840.
(45) Song, L.; Zhang, Y.-J.; Chen, X.; Li, S.; Lu, H.-Z.; Wu, C.-S.; Tan, Z.-H.; Liu, W.-Y.; Shi, X.-M. Water relations and gas exchange of fan bryophytes and their adaptations to microhabitats in an Asian subtropical montane cloud forest. *J. Plant Res.* **2015**, *128*, 573−584.
(46) Finnigan, J. The storage term in eddy flux calculations. *Agric. For. Meteorol.* **2006**, *136*, 108−113.
(47) Blum, J. D.; Bergquist, B. A. Reporting of variations in the natural isotopic composition of mercury. *Anal. Bioanal. Chem.* **2007**, *388*, 353−359.
(48) Sommar, J.; Zhu, W.; Shang, L.; Lin, C.-J.; Feng, X. Seasonal variations in metallic mercury (Hg^0) vapor exchange over biannual

https://doi.org/10.1021/acs.est.2c00778
Environ. Sci. Technol. 2022, 56, 5950−5959

wheat−corn rotation cropland in the North China Plain. *Biogeosciences* **2016**, *13*, 2029−2049.
(49) Sommar, J.; Zhu, W.; Shang, L.; Feng, X.; Lin, C.-J. A whole-air relaxed eddy accumulation measurement system for sampling vertical vapour exchange of elemental mercury. *Tellus, Ser. B: Chem. Phys. Meteorol.* **2013**, *65*, 19940.
(50) Zhu, W.; Sommar, J.; Lin, C.-J.; Feng, X. Mercury vapor air−surface exchange measured by collocated micrometeorological and enclosure methods − Part II: Bias and Uncertainty Analysis. *Atmos. Chem. Phys.* **2015**, *15*, 5359−5376.
(51) Kamp, J.; Skov, H.; Jensen, B.; Sørensen, L. L. Fluxes of gaseous elemental mercury (GEM) in the High Arctic during atmospheric mercury depletion events (AMDEs). *Atmos. Chem. Phys.* **2018**, *18*, 6923−6938.
(52) Osterwalder, S.; Fritsche, J.; Alewell, C.; Schmutz, M.; Nilsson, M. B.; Jocher, G.; Sommar, J.; Rinne, J.; Bishop, K. A dual-inlet, single detector relaxed eddy accumulation system for long-term measurement of mercury flux. *Atmos. Meas. Tech.* **2016**, *9*, 509−524.
(53) Schade, G. W.; Goldstein, A. H. Fluxes of oxygenated volatile organic compounds from a ponderosa pine plantation. *J. Geophys. Res.: Atmos.* **2001**, *106*, 3111−3123.
(54) Foken, T. *Micrometeorology*; Springer-Verlag, 2008.
(55) Sprovieri, F.; Pirrone, N.; Bencardino, M.; D'Amore, F.; Carbone, F.; Cinnirella, S.; Mannarino, V.; Landis, M.; Ebinghaus, R.; Weigelt, A.; Brunke, E.-G.; Labuschagne, C.; Martin, L.; Munthe, J.; Wängberg, I.; Artaxo, P.; Morais, F.; Barbosa, H. d. M. J.; Brito, J.; Cairns, W.; Barbante, C.; Diéguez, M. d. C.; Garcia, P. E.; Dommergue, A.; Angot, H.; Magand, O.; Skov, H.; Horvat, M.; Kotnik, J.; Read, K. A.; Neves, L. M.; Gawlik, B. M.; Sena, F.; Mashyanov, N.; Obolkin, V.; Wip, D.; Feng, X. B.; Zhang, H.; Fu, X.; Ramachandran, R.; Cossa, D.; Knoery, J.; Marusczak, N.; Nerentorp, M.; Norstrom, C. Atmospheric mercury concentrations observed at ground-based monitoring sites globally distributed in the framework of the GMOS network. *Atmos. Chem. Phys.* **2016**, *16*, 11915−11935.
(56) Wang, X.; Zhang, H.; Lin, C. J.; Fu, X.; Zhang, Y.; Feng, X. Transboundary transport and deposition of Hg emission from springtime biomass burning in the Indo-China Peninsula. *J. Geophys. Res.: Atmos.* **2015**, *120*, 9758.
(57) Yu, B.; Fu, X.; Yin, R.; Zhang, H.; Wang, X.; Lin, C.-J.; Wu, C.; Zhang, Y.; He, N.; Fu, P.; Wang, Z.; Shang, L.; Sommar, J.; Sonke, J. E.; Maurice, L.; Guinot, B.; Feng, X. Isotopic Composition of Atmospheric Mercury in China: New Evidence for Sources and Transformation Processes in Air and in Vegetation. *Environ. Sci. Technol.* **2016**, *50*, 9262−9269.
(58) Kurz, A. Y.; Blum, J. D.; Gratz, L. E.; Jaffe, D. A. Contrasting Controls on the Diel Isotopic Variation of Hg0 at Two High Elevation Sites in the Western United States. *Environ. Sci. Technol.* **2020**, *54*, 10502−10513.
(59) Yu, B.; Yang, L.; Wang, L.; Liu, H.; Xiao, C.; Liang, Y.; Liu, Q.; Yin, Y.; Hu, L.; Shi, J.; Jiang, G. New evidence for atmospheric mercury transformations in the marine boundary layer from stable mercury isotopes. *Atmos. Chem. Phys.* **2020**, *20*, 9713−9723.
(60) Yuan, W.; Wang, X.; Lin, C.-J.; Sommar, J. O.; Wang, B.; Lu, Z.; Feng, X. Quantification of Atmospheric Mercury Deposition to and Legacy Re-emission from a Subtropical Forest Floor by Mercury Isotopes. *Environ. Sci. Technol.* **2021**, *55*, 12352.
(61) Zhu, W.; Sommar, J.; Lin, C.-J.; Feng, X. Mercury vapor air−surface exchange measured by collocated micrometeorological and enclosure methods − Part I: Data comparability and method characteristics. *Atmos. Chem. Phys.* **2015**, *15*, 685−702.
(62) Yuan, W.; Wang, X.; Lin, C.-J.; Sommar, J.; Lu, Z.; Feng, X. Process factors driving dynamic exchange of elemental mercury vapor over soil in broadleaf forest ecosystems. *Atmos. Environ.* **2019**, *219*, 117047.
(63) Lindberg, S. E.; Dong, W.; Meyers, T. Transpiration of gaseous elemental mercury through vegetation in a subtropical wetland in Florida. *Atmos. Environ.* **2002**, *36*, 5207−5219.
(64) Lindberg, S. E.; Meyers, T. P.; Taylor, G. E.; Turner, R. R.; Schroeder, W. H. Atmosphere-surface exchange of mercury in a forest - results of modeling and gradient approaches. *J. Geophys. Res.: Atmos.* **1992**, *97*, 2519−2528.
(65) Laacouri, A.; Nater, E. A.; Kolka, R. K. Distribution and uptake dynamics of mercury in leaves of common deciduous tree species in Minnesota, U.S.A. *Environ. Sci. Technol.* **2013**, *47*, 10462−10470.
(66) Siwik, E. I. H.; Campbell, L. M.; Mierle, G. Fine-scale mercury trends in temperate deciduous tree leaves from Ontario, Canada. *Sci. Total Environ.* **2009**, *407*, 6275−6279.
(67) Wohlgemuth, L.; Osterwalder, S.; Joseph, C.; Kahmen, A.; Hoch, G.; Alewell, C.; Jiskra, M. A bottom-up quantification of foliar mercury uptake fluxes across Europe. *Biogeosciences* **2020**, *17*, 6441−6456.
(68) Howard, D.; Edwards, G. C. Mercury fluxes over an Australian alpine grassland and observation of nocturnal atmospheric mercury depletion events. *Atmos. Chem. Phys.* **2018**, *18*, 129−142.
(69) Lindqvist, O.; Johansson, K.; Bringmark, L.; Timm, B.; Aastrup, M.; Andersson, A.; Hovsenius, G.; Håkanson, L.; Iverfeldt, k.; Meili, M. Mercury in the Swedish Environment - Recent Research on Causes, Consequences and Corrective Methods. *Water, Air, Soil Pollut.* **1991**, *55*, xi−261.
(70) Risch, M. R.; DeWild, J. F.; Gay, D. A.; Zhang, L.; Boyer, E. W.; Krabbenhoft, D. P. Atmospheric mercury deposition to forests in the eastern USA. *Environ. Pollut.* **2017**, *228*, 8−18.
(71) Yu, Q.; Luo, Y.; Xu, G.; Wu, Q.; Wang, S.; Hao, J.; Duan, L. Subtropical Forests Act as Mercury Sinks but as Net Sources of Gaseous Elemental Mercury in South China. *Environ. Sci. Technol.* **2020**, *54*, 2772−2779.
(72) Harris, N. L.; Gibbs, D. A.; Baccini, A.; Birdsey, R. A.; de Bruin, S.; Farina, M.; Fatoyinbo, L.; Hansen, M. C.; Herold, M.; Houghton, R. A.; Potapov, P. V.; Suarez, D. R.; Roman-Cuesta, R. M.; Saatchi, S. S.; Slay, C. M.; Turubanova, S. A.; Tyukavina, A. Global maps of twenty-first century forest carbon fluxes. *Nat. Clim. Change* **2021**, *11*, 234−240.
(73) Blackwell, B. D.; Driscoll, C. T. Using foliar and forest floor mercury concentrations to assess spatial patterns of mercury deposition. *Environ. Pollut.* **2015**, *202*, 126−134.
(74) Zhou, J.; Du, B.; Shang, L.; Wang, Z.; Cui, H.; Fan, X.; Zhou, J. Mercury fluxes, budgets, and pools in forest ecosystems of China: A review. *Crit. Rev. Environ. Sci. Technol.* **2019**, *50*, 1411−1450.
(75) Luo, Y.; Duan, L.; Driscoll, C. T.; Xu, G.; Shao, M.; Taylor, M.; Wang, S.; Hao, J. Foliage/atmosphere exchange of mercury in a subtropical coniferous forest in south China. *J. Geophys. Res.: Biogeosci.* **2016**, *121*, 2006−2016.
(76) Yuan, W.; Wang, X.; Lin, C. J.; Zhang, H.; Feng, X.; Lu, Z. Impacts of Extreme Weather on Mercury Uptake and Storage in Subtropical Forest Ecosystems. *J. Geophys. Res.: Biogeosci.* **2022**, *127*, e2021JG006681. DOI: 10.1029/2021JG006681.
(77) de Jong, W.; Liu, J.; Youn, Y.-C. Land and forests in the Anthropocene: Trends and outlooks in Asia. *For. Pol. Econ.* **2017**, *79*, 17−25.
(78) Hsu-Kim, H.; Eckley, C. S.; Achá, D.; Feng, X.; Gilmour, C. C.; Jonsson, S.; Mitchell, C. P. J. Challenges and opportunities for managing aquatic mercury pollution in altered landscapes. *Ambio* **2018**, *47*, 141−169.

https://doi.org/10.1021/acs.est.2c00778
Environ. Sci. Technol. 2022, 56, 5950−5959